Wetting of adhesive fluid controls insect adhesion in air and underwater

Pranav Sudersan,[†] Michael Kappl,[†] Bat-El Pinchasik,[‡] Hans-Jürgen Butt,[†] and Thomas Endlein[*,†]

[†]Max Planck Institute for Polymer Research, Ackermannweg 10, 55128 Mainz, Germany

[‡]School of Mechanical Engineering, Tel Aviv University, Tel Aviv-Yafo, Israel

E-mail: endlein01@mpip-mainz.mpg.de

Phone: +49 6131 379 111. Fax: +49 6131 379 310

Abstract

Insects like beetles can stick to various surfaces using hairy pads on their legs. It was previously shown that these pads can even attach underwater, presumably due to an air bubble trapped around the pad. However, the bubble's contribution to adhesion via capillary force remained unclear. To investigate the role of the bubble, we measured *in-vivo* underwater adhesion of a ladybug's pad, in the presence and absence of the trapped bubble and compare it with its adhesion in air. Our experiments reveal that on a hydrophobic substrate, even without a bubble, the pad can show adhesion underwater comparable to that in air. On a hydrophilic substrate, underwater adhesion is significantly reduced, with or without a trapped bubble. To explain these results, we develop a simple theoretical model for the net adhesion of a hairy pad due to capillary forces. Our results demonstrate that the wetting properties of the adhesive fluid determines the insect's adhesion in both air and underwater conditions.

1 Introduction

The question of how insects and other small animals can walk on smooth surfaces against gravity has fascinated scientists for at least the past three centuries[?][?]. We now know that such animals are able to adhere by using specialized organs on their feet called adhesive pads. These adhesive pads exist in a variety of types depending on the animal, but are generally categorized into: 1) "smooth pads" found in ants[?], stick insects[?], etc. and 2) "hairy pads" seen in flies[?], geckos[?] and others. The hairy pads show: 1) compliance to rough surfaces due to their lower effective modulus, 2) angle dependent adhesion due to asymmetric hair geometry and 3) self-cleaning capability[?], which makes them suitable to adhere to most surfaces reversibly. Many of these insects pads also secrete an adhesive fluid, as seen in flies and ants[?] ("wet adhesion"), while others such as spiders and geckos rely on their dry hairy pads for attachment ("dry adhesion"). In the "wet adhesion" case, fluid secretion can enforce adhesion through surface tension and viscous forces[?], while, "dry adhesion" relies mostly on van der Waals forces[?].

Terrestrial beetles such as the dock beetle or the ladybug have hairy pads consisting of a dense array of hair-like structures called setae. The setae tips can be discoidal, spatula or pointed shaped, which are distributed throughout the pad depending on sex or species[?]. Single seta force measurements revealed that discoidal shaped seta shows larger pull-off force than spatula and pointed setae[?], illustrating the role of hair geometry in adhesion. The tip of each seta secretes approximately one femtoliter of oily adhesive fluid[?]. The fluid's chemical composition is identified as a mixture of mostly long chain hydrocarbons[?] with traces of triglycerides, fatty acids and cholesterol[?][?]. A recent study by Gernay et. al.[?], based on an elastocapillary model, has been able to reasonably predict single seta adhesion forces theoretically, confirming the dominant role of surface tension in the "wet adhesion" of beetles.

While most of the studies on insect adhesion are done under natural conditions in air, insect attachment underwater has been relatively unexplored. Typically, underwater adhesion

is complicated to achieve due to the difficulty in displacing the water layer and enable good contact[?]. Regardless, a study on leaf beetles[?] has revealed that they can in fact attach quite well to surfaces underwater. Its hairy pad traps an air bubble underwater, which dewets the surface on contact. It has been hypothesized that a combination of capillary forces due the air bubble and hair secretions within the dewetted area results in its adhesion underwater. However, a detailed investigation of the bubble's contribution and necessity to adhere to different surfaces is lacking. Geckos are also known to adhere underwater, where its shear adhesion force on hydrophobic substrates are similar in both air and underwater conditions. Interestingly, its adhesion on a fluorinated substrate is even larger underwater than in air[?]. This has been partially explained by a thermodynamic work of adhesion model, assuming full displacement of water at the interface, leading to a dry "van der Waals" contact of hairs with the surface[?].

The goal of this paper is to provide a generalized picture of adhesion for insects which use hairy pads and secrete a oily fluid for attachment. First, we measured adhesion of a single constrained pad of a live ladybug beetle in air and underwater conditions, both on smooth hydrophilic and hydrophobic glass surfaces, with a microscopic observation of the contact process. Second, we developed a simple theoretical model considering capillary forces to predict the net adhesion force of a hairy pad under different conditions. The case of underwater adhesion was studied both in the presence and absence of a trapped bubble, to decouple the bubble's role in the insect's adhesion. Finally, we discuss key insights gained from our experiments and model with regards to understanding adhesion in other animals.

2   Experimental

Normal adhesion force measurements on a restrained leg of a live ladybug beetle were performed. We characterize adhesion by the pull-off force during detachment. Measurements were done against smooth glass and fluorinated surfaces to represent hydrophilic and hy-

drophobic substrates respectively. When no water was present, we labeled the contact type as "*in air*". For the underwater conditions, measurements were done both in the presence and absence of a trapped bubble ("*underwater: bubble*" and "*underwater: no bubble*", respectively) to investigate the bubble's role in underwater adhesion. Adhesion force for each of the labeled contact types were compared for both substrates.

2.1 Material and Methods

2.1.1 Insect preparation

Seven-spotted male adult ladybug beetles (*Coccinella septempuctata*) purchased from Katz Biotech (Baruth, Germany) were used for adhesion tests. The beetles were housed in a plastic box filled with leaves, twigs and stones at room temperature and 60-80% relative humidity with daily access to sunlight. They were fed with raisins, honey and water *ad libitum*.

Each leg of the beetle has a pair of hairy pads covered with mostly discoidal shaped setae, capable of strong adhesion. For the test, we only allowed the distal-end pad to make contact. The beetle's leg was constrained similar to the method described by Bullock et al[?] . A steel ball fixed with a piece of thick solder wire served as a rotatable holder to fix the beetle and align its leg (Figure **??**). The beetle was first anesthetized using CO_2 sublimating from a piece of dry ice and then glued to the steel ball on its back. Its front left leg was carefully fixed to the solder wire of the holder using Blue-Tac. Its claws were fixed using epoxy glue to prevent any wiggling. A small piece of non-sticky Teflon tape helped to keep its other legs tucked close to the body and avoid their interference during the adhesion test.

After measurements, the beetle was freed by carefully removing the epoxy glue and Blue-Tac without harming it and set free.

2.1.2 Substrate preparation

Standard 20 mm wide glass coverslips were used as the hydrophilic substrate. Glass was wiped with isopropanol, rinsed in water and dried under nitrogen flow. The surface was then plasma cleaned in a oxygen plasma chamber (Diener Electronic Femto) for 10 min at 120 W. The surface was further rinsed with water and dried under nitrogen flow.

For the hydrophobic substrate, the glass cover slip was coated with a fluorosilane via chemical vapor deposition (CVD). First, the glass was cleaned using IPA and plasma treated as before. Next, 0.2 ml of Trichloro(1H,1H,2H,2H-perfluorooctyl) silane (PFOTS), procured from Sigma Aldrich, was put in a sealed chamber along with the the cleaned glass. The chamber was placed under 100 mbar pressure for 10 min for the CVD process. Finally, the substrate was annealed at 150℃ for 3 hours.

The substrate wettability was characterized by dynamic contact angle measurements, performed with a DataPhysics OCA 35 contact angle goniometer. Milli-Q water and n-hexadecane were used as test liquids. Advancing and receding contact angles were measured for a maximum drop volume of 10 μl and with 0.5 μl/s flow rate.

Table 1: Dynamic contact angles measurements

Substrate	Liquid	θ_A	θ_R
Glass	Water	$63\pm5°$	$20\pm2°$
	n-Hexadecane	$<10°$	$<10°$
PFOTS	Water	$122\pm1°$	$93\pm2°$
	n-Hexadecane	$88\pm2°$	$56\pm5°$

2.1.3 Adhesion test

Adhesion measurements were performed on a custom force measurement setup developed in-house (Figure **??**). A fiber optic displacement sensor (*Philtec D20, PHILTEC, Inc. USA*) together with a steel bending beam (spring constant = 68.1 N/m) constitutes the vertical force sensor. Beam deflection was calibrated using 4 different known weights to get the corresponding force. A plastic 3D printed substrate holder was glued to the end of the

bending beam. The holder was designed to enable switching from one substrate to another without removing any glue. It also had transparent side walls which allowed us to fill it with water for the underwater experiments as well as observe the contact. The sensor was mounted on a stage consisting of a X-piezo, used for precise lateral movements, XYZ motors, for coarse movements and a goniometer, for adjusting substrate alignment with the optics. Additionally, a separate Z-piezo, fixed upright, was used for vertical up-down motion, bringing the insect in contact with the substrate from the top. A 3 axis manual micro-manipulator together with the rotatable steel ball allowed good alignment of the beetle's foot to the substrate. A coaxial illuminated tube microscope (*Navitar*) with 2× objective and a stereo-microscope with 1× objective (*Wild Heerbrugg*) fit with cameras were used to record the sample contact with the substrate from ventral and side views respectively. Pad contact area was visualized through the substrate in total reflection mode by the ventral view camera. The data acquisition from the force sensor and cameras, together with the appropriate piezo motion steps were synchronized using a custom LABVIEW program. Force data was acquired at a sample rate of 984 Hz, averaged to 512 points per motion step. Videos were recorded at 20 frames per second.

The vertical and lateral piezos were together used to perform approach-retract adhesion tests with the substrate to get the pull-off force. However, instead of a simple down-up motion, some additional motion steps were included (Figure **??**). A 100 µm lateral sliding motion was done after the leg makes contact, to give it a proximal pull which will orient its hairs with the substrate[?] . An additional 10 µm compression step (approach) was done to ensure all hairs were loaded in compression and made good contact with the surface. A short pause (1 s) was introduced to minimize any viscoelastic effects before finally retracting the leg away from the substrate. All approach, retract and lateral slide motion was done at a speed of 62.5 µm/s. Ventral view video recordings were used for contact area extraction while the side view imaging was used to visually aid orienting the pad with the substrate before a test.

For underwater experiments, 1 ml Milli-Q water was pipetted into the substrate holder. In order to achieve an underwater contact without a trapped air bubble, the water was first degassed in a vacuum chamber at 10 mbar pressure for 3 hours and used immediately. Before experiment, the pad was repeatedly brought into contact with the surface 10 times to equilibriate the pad system. 5 force measurements were subsequently performed on a fresh spot of the substrate and averaged for data analysis. Experiments were repeated with 5 individual beetles for each type of contact and substrate. In total, 30 beetles were tested.
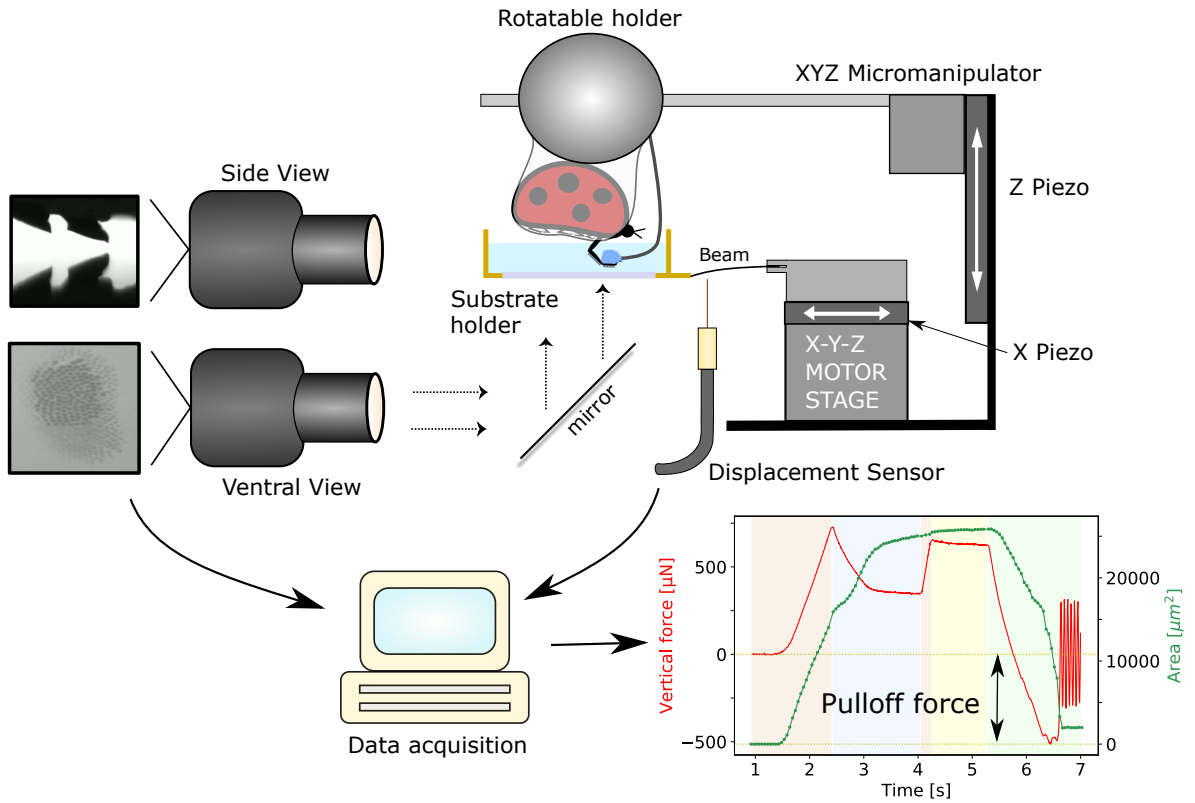

Figure 1: Adhesion test setup. The recorded force data and contact area of distal pad are shown in the plot, in which, the shaded regions represent distinct piezo motion steps, negative force values represent attraction and the minimum force peak during the final retraction step is the adhesion force.

2.1.4 Field desorption mass spectroscopy

A previous study on archanids[?] reported that its secreted fluid does not dissolve in water. To confirm if even the beetle retains its adhesive fluid underwater, we perform Field Desorption Mass Spectroscopy (FDMS) using a ZAB 2-SE-FPD spectrometer (VG Instruments). The measurements were done on the extracted secretions before and after rinsing its legs with water. The middle leg of an Asian ladybird (*Harmonia axyridis*) was immersed in 50 µL THF for 20 min and then transferred to the measurement chamber of the FDMS. As a reference, pure THF was used. The second middle leg of the same ladybird was subsequently immersed in 100 µL Milli-Q water for 15 min, then in THF for 20 min and then transferred to the measurement chamber of the spectrometer. Molecular composition was extracted from the peak positions of the FDMS spectra.

2.1.5 Data analysis

Extraction of pull-off force from force data, image processing, plotting and statistical analysis were all performed in "*Buggee*", a tool written in Python using open-source libraries for synchronous analysis of force data and video recordings (`https://github.com/PranavSudersan/Buggee`).

For measurements in air, the pull-off force was defined as the minimum negative force during the final retraction step (Figure **??**). For underwater measurements, an additional correction was necessary. When the beetle was submerged underwater, its contact line at the water surface shifted, which influenced the force readout due to surface tension effects. This effect needed to be canceled. So, a "background" force data was recorded, where the submerged beetle makes no contact with the substrate. This background data was then subtracted from a typical force data with substrate contact to correct for the external surface tension effects. The pull-off force was subsequently calculated from the minima as before.

Data sets were compared for statistical differences using pairwise Student t-test and their corresponding p-value and Common Language Effect Size (CLES) are reported. Shapiro-

Wilk test was done for each data set to verify a normal distribution of its residuals and Levene's test was done to check for variance homogeneity, to validate the t-test assumptions. Bonferroni's correction was used to account for multiple comparison between groups.

2.2 Results

2.2.1 Adhesion measurements

In air, adhesion forces of the distal pad of ladybug beetle against glass and PFOTS are rather similar; no significant differences are detected (Figure **??** and Table **??**). In contrast, underwater adhesion on PFOTS surface is significantly larger than on glass ($p < 0.001$). This stronger adhesion on PFOTS is observed both in the presence and absence of a trapped bubble. In both cases, adhesion force reach similar values as in air. In contrast, on glass, adhesion underwater is significantly reduced as compared to dry conditions, irrespective of the presence of a trapped bubble ($p \leq 0.002$). Underwater adhesion on glass tends to be slightly higher in the presence of a bubble (CLES = 0.84). However, this difference is small and not statistically significant ($p = 0.07$).
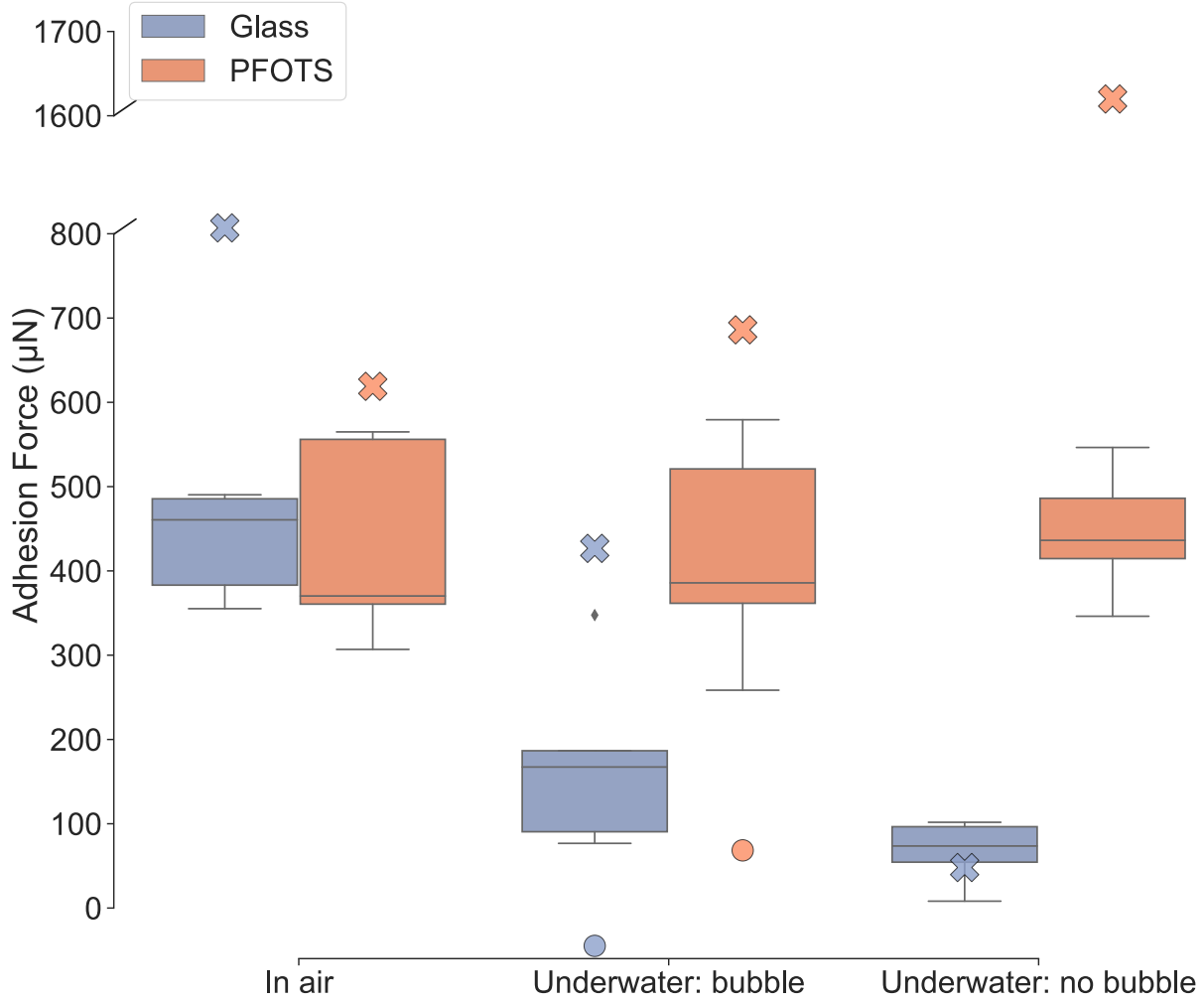
Figure 2: Box-and-whisker plot showing single leg adhesion force measurements of ladybug beetle (*Coccinella septempuctata*) on glass and PFOTS substrates in air and underwater conditions. The two types of contact during underwater experiments are represented separately: "*bubble*" and "*no bubble*". Crosses represent theoretical predictions of adhesion force, while, circles represent the contribution of the bubble itself, calculated from the capillary bridge model. In the model, hair diameter = 4 μm, pad diameter = 200 μm, hair height = 40 μm, N_{hairs} = 500, V_{fluid} = 4.2 fL and V_{bubble} = 1.2 nL. Interfacial tension of the adhesive fluid in air and water were assumed to be 24 mN/m and 48 mN/m respectively and water surface tension is 72 mN/m.

Apart from the three depicted contact types, we observed an additional fourth type which occurred in roughly 25% of our underwater experiments. In this scenario, the ventral view recordings show that the hairs did not appear to contact well with the substrate, unlike the other three contact types. This "bad contact" scenario shows no adhesion with either glass

or PFOTS substrate. While it was not completely clear why such a contact occurs, there can be two possible reasons. First, the hairs could get bundled due to a small air meniscus within the hairs, resulting in their disorientation. Second, a thin water layer at the substrate interface might not be drained out to allow the hairs to make contact with the substrate, resulting in a loss of adhesion.

2.2.2 Field desorption mass spectroscopy

FDMS results confirm the presence of adhesive fluid on an Asian ladybird's leg when underwater (Table **??**). Molecular weights of the secreted fluid mixtures extracted from the beetle's leg, without and after immersion in water, show that, except for two molecular weights (406.8 g/mol and 331.6 g/mol), the chemical fingerprint remained unchanged This indicates that the adhesion fluid was not washed away underwater. Probable compounds in the fluid, corresponding to the resultant molecular weights, include mostly aliphatic hydrocarbons with traces of aldehydes.

Table 2: Molecular weights of adhesive fluid secretion of *Harmonia axyridis* with and without rinsing the beetle's leg in water. Molecular weights were extracted from the peaks in the FDMS spectra.

Without rinsing (g/mol)	After rinsing (g/mol)	Probable compounds
324.5	324.5	$C_{23}H_{48}$, $C_{22}H_{44}O$
	331.6	$C_{24}H_{44}$
350.5	350.5	$C_{25}H_{50}$
352.5	352.5	$C_{25}H_{52}$, $C_{24}H_{48}O$
378.5	378.5	$C_{27}H_{54}$
404.6	404.5	$C_{29}H_{56}$
406.8		$C_{29}H_{58}$
432.8	432.7	$C_{31}H_{60}$

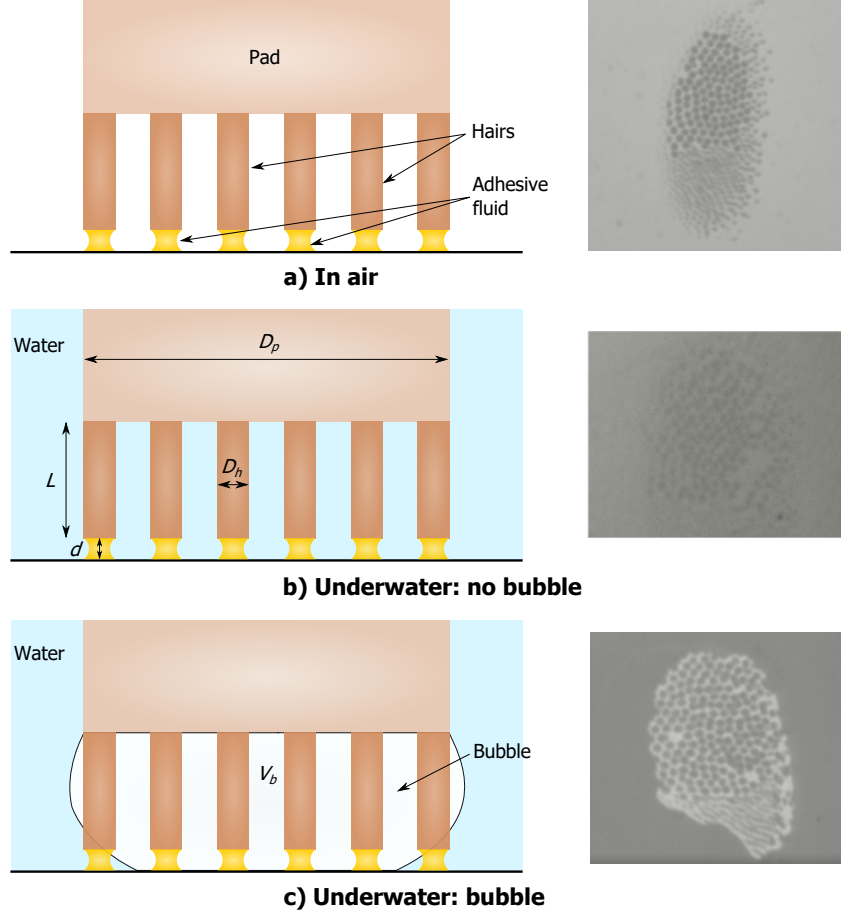# 3 Theory

3.1 Capillary Bridge Model

Figure 3: The capillary bridge model. The hairs make contact with the substrate in three ways: a) *In air*, where the adhesive fluid bridges are surrounded by air; b) *Underwater: no bubble*, where the adhesive fluid bridges are fully surrounded by water; c) *Underwater: bubble*, where part of the adhesive fluid bridges are inside the bubble while others are outside in water. The corresponding ventral view contact images of the beetle's pad are shown on the right.

We model the hairy pad as an array of N cylindrical rods of length, L, and diameter, D_h, fixed to a flat circular pad of diameter, D_p (Figure **??**). The hairs and the pad are assumed to be perfectly rigid, for simplicity. The tip of each hair has an adhesive fluid of volume, V_f, making contact with the substrate. The fluid is pinned to the circumference of the hair and

forms a capillary bridge of height, d. Similar to our experiments, we consider three types of contacts for the pad: 1) *In air*, 2) *Underwater: no bubble* and 3) *Underwater: bubble*. In the third case, a bubble of volume, V_b, is trapped between the hairs and pinned to the pad circumference.

To characterize the adhesive fluid and bubble volume we define two radii, s_f and s_b, respectively, by $V_f = \frac{4}{3}\pi s_f^3$ and $V_b = \frac{4}{3}\pi s_b^3$. Here, s_f and s_b are the radii of spheres with equivalent volumes. Fluid and bubble radii are assumed to scale proportional to their corresponding pinned contact diameter. We thus defined the size parameters, $\phi_f = D_h/(2s_f)$ and $\phi_b = D_p/(2s_b)$ for the fluid and bubble respectively, to conveniently scale their volumes relative to the hair and pad diameters they were pinned to.

The net force for cases 1 and 2 can be calculated as:

$$F_{net} = Nf \tag{1}$$

Here, f is the capillary force of a single fluid bridge at a distance, d, in air (f_{air}) or underwater (f_{water}).

For case 3, the net force is given by:

$$F_{net} = N_{in}f_{air} + N_{out}f_{water} + f_{bubble} \tag{2}$$

Here, N_{in} and N_{out} are the number of hairs inside and outside the bubble, respectively, f_{air} and f_{water} are the capillary forces of the fluid bridge inside and outside the bubble, respectively, and f_{bubble} is the capillary force contribution due to the bubble meniscus alone at distance $d + L$.

The capillary force, f, is the sum of two contributions: surface tension and Laplace pressure (equation **??**). Force versus distance for a single capillary bridge is calculated by Surface Evolver simulations[?] , (described in **??**) and used to obtain F_{net} as a function of d for each type of contact. The adhesion force of the complete hairy pad system is then

obtained from the minima of F_{net}, where negative force values represent attraction.

We have considered f_{air} and f_{water} to be distinct terms because the capillary force by the adhesive fluid will be different in air and underwater due to its different contact angle and interfacial tension in each case. Using the Young-Duprè equations for each case of fluid-air, fluid-water and water-air interface, one can derive the following relation for the contact angle of the adhesive fluid underwater:

$$\cos\theta_{fw} = \frac{\gamma_{fa}\cos\theta_{fa} - \gamma_{wa}\cos\theta_{wa}}{\gamma_{fw}} \tag{3}$$

Here, θ_{fw} and θ_{fa} are the contact angles of the adhesive fluid with the substrate in water and air respectively, θ_{wa} is the contact angle of water with the substrate in air, γ_{fa} is the surface tension of the adhesive fluid, γ_{wa} is the surface tension of water and γ_{fw} is the interfacial tension of the adhesive fluid with water.

All lengths are normalized w.r.t. s_f and forces are normalized w.r.t. $\gamma_{fa}s_f$. Interfacial tension values are fixed relative to γ_{fa}. Non dimensional bubble volume is expressed as, $\hat{V}_b = V_b/s_f^3$

Geometric parameters and interfacial properties are kept fixed for all model calculations (Table ??). Here, we assume the adhesive fluid to be an oil-lke substance and thus the interfacial tension ratios γ_{wa}/γ_{fa} and γ_{fw}/γ_{fa} are taken corresponding to typical values of oil and water. We consider representative hydrophilic and hydrophobic substrates with θ_{fa} and θ_{wa} values corresponding to a typical glass and fluorinated surface, respectively. Area fraction of the hairs relative to the pad, $\alpha = ND_h^2/D_p^2$, hair aspect ratio, L/D_h, and fluid size parameter, ϕ_f, are fixed to values typical for a ladybug's hairy pad.

First, we calculate force-distance curves for a single pinned liquid capillary bridge. Second, the effect of substrate on the force-distance curves of the hairy pad system is compared for each type of contact. Third, the effect of varying hair diameter, D_h, on net adhesion is studied. Finally, we look at the effect of changing the bubble volume, $\hat{V}_b$, on the net underwater adhesion.

Table 3: Fixed parameters of the capillary bridge model

Property	Value
Area fraction, α	0.1
Hair aspect ratio, L/D_h	10
Water surface tension ratio, γ_{wa}/γ_{fa}	3
Fluid-water interfacial tension ratio, γ_{fw}/γ_{fa}	2
Fluid size parameter, ϕ_f	2
Hydrophilic substrate	$\theta_{fa} = 6°$, $\theta_{wa} = 24°$
Hydrophobic substrate	$\theta_{fa} = 50°$, $\theta_{wa} = 120°$

3.2 Capillary force of a pinned liquid bridge

Forces due to a single pinned capillary liquid bridge in contact with a substrate are obtained via Surface Evolver simulations (Figure ??). We see that, generally, the shape of the liquid meniscus determines the strength of its adhesion force. High adhesion is seen for contact angles less than $\sim 70°$ due to a net negative curvature of the meniscus, while low adhesion is seen for contact angles greater than $\sim 150°$ due to its net curvature being close to zero. The Laplace pressure contribution to the net adhesion force dominates for contact angles less than $100°$ (Figure ??b). Interestingly, its contribution to the adhesion force is mostly non-repulsive for contact angles greater than $90°$. This is because, the low volume of the liquid and its pinned contact line prevents the meniscus from having a high positive curvature due to geometric constraints. Only for a contact angle of $150°$, the liquid's curvature becomes positive, manifested in its slightly repulsive Laplace contribution. Surface tension makes a significant contribution to the net force only for a small range of contact angles close to $90°$. For contact angles greater than $150°$, the net adhesion force approaches zero.
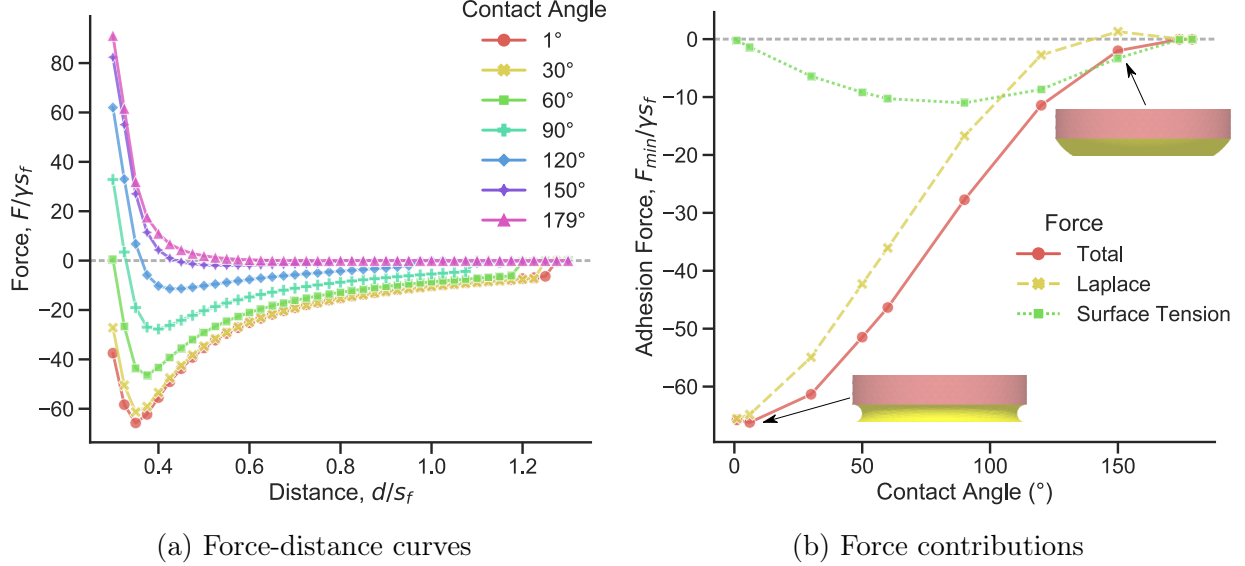
(a) Force-distance curves

(b) Force contributions

Figure 4: Normalized capillary force of a single liquid bridge in contact with a substrate and pinned to a circular perimeter on top. Fluid size parameter, $\phi_f = 2$. Negative force values represents attraction. a) Force-distance curves are shown for different contact angles of the liquid with the substrate. b) Adhesion forces, calculated from the minima of the corresponding force-distance curves, are plotted as a function of contact angle with the substrate, together with its Laplace and surface tension components (equation **??**). Simulation snapshots of the liquid meniscus corresponding to angles 6° and 150° are depicted.

The force-distance curves show a general trend of being repulsive at small distances (Figure **??**a). This is a result of the pinned contact line on the top. A limited volume is available for the liquid to occupy when the gap distance is small, causing the meniscus shape to bulge outwards near the pinned contact line. This creates a net positive curvature, resulting in a positive Laplace pressure and thus repulsion. Without pinning, the capillary forces would have shown high attractive forces on a hydrophilic substrate[?] .

3.3   Effect of the substrate

The normalized force-distance curves of a hairy pad system on a hydrophilic and hydrophobic substrate are predicted based on the capillary bridge model and compared for the different contact types (Figure **??**). The forces in each case are calculated from equations (**??**) and (**??**) for fixed geometric and interfacial properties (Table **??**).

16

On the hydrophilic substrate ($\theta_{wa} = 24°$), highest adhesion is seen when the hairs contact in air, while lowest adhesion occurs underwater without a trapped bubble. The presence of a bubble leads to intermediate force values. In contrast, on a hydrophobic substrate ($\theta_{wa} = 120°$), highest adhesion is seen for the underwater case without a trapped bubble, much larger than in air. When a bubble is present, the forces are only slightly larger than in air.
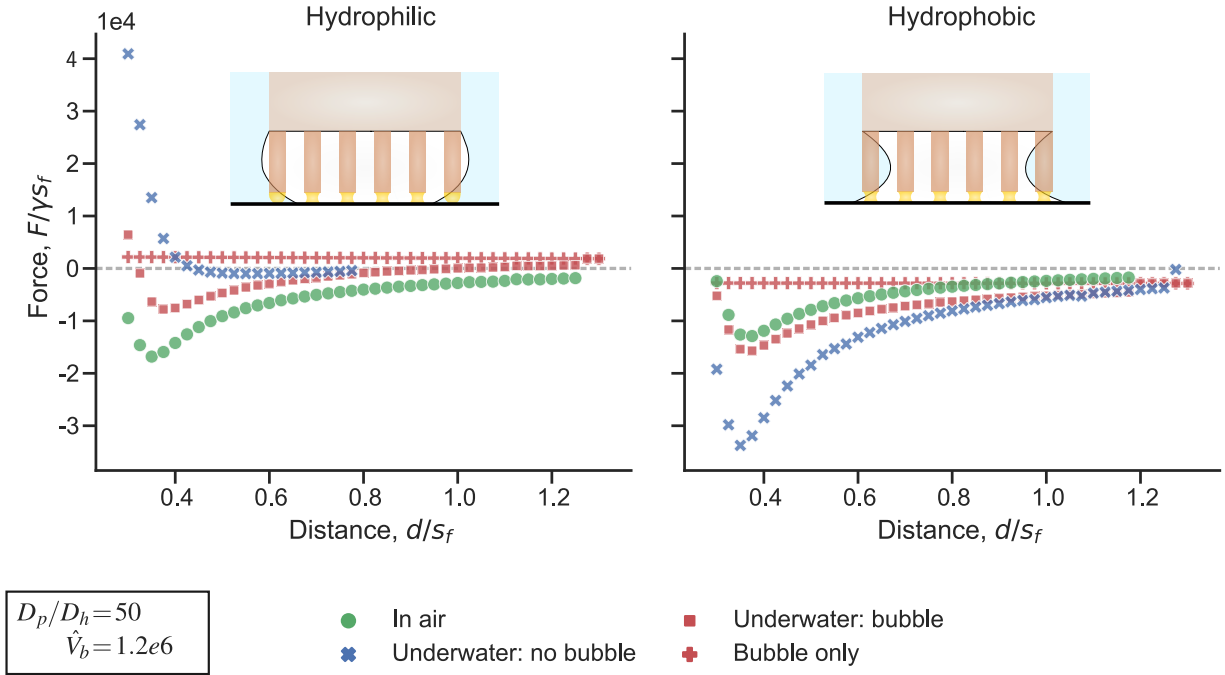

Figure 5: Theoretical force-distance curves of a hairy pad system on a hydrophilic and hydrophobic substrate in air and underwater conditions. A negative force value represents attraction. Normalized forces are calculated from the capillary bridge model, with model parameters listed in Table **??**. The bubble's contribution to the net force for an *underwater: bubble* contact is denoted by plus symbols. Insets represent the *underwater: bubble* contact for each substrate.

The observed trend in forces can be explained by how the adhesive fluid wets the surface in each case. On a hydrophilic substrate, the contact angle of the oily adhesive fluid is 6°, when surrounded by air (Table **??**) and 150°, when surrounded by water (equation (**??**)). This results in the meniscus shape to have a net negative and slightly positive curvatures, respectively, resulting in strong adhesion in air and poor adhesion underwater. On a hy-

drophobic substrate however, the contact angles of the fluid in air and water are 50° and 1°, respectively. In both cases, the contact angles are low, resulting in strong adhesion in both media. Additionally, the interfacial tension of the oily fluid underwater (γ_{fw}) is twice that of in air (γ_{fa}). Thus, we see a higher capillary adhesion for the *underwater: no bubble* case when compared to *in air* (Figure **??**). Note that the contact area is fixed in all cases by keeping the area fraction and D_p/D_h constant. Thus the observed effects is not a result of changing contact area, but rather on the nature of capillary forces.
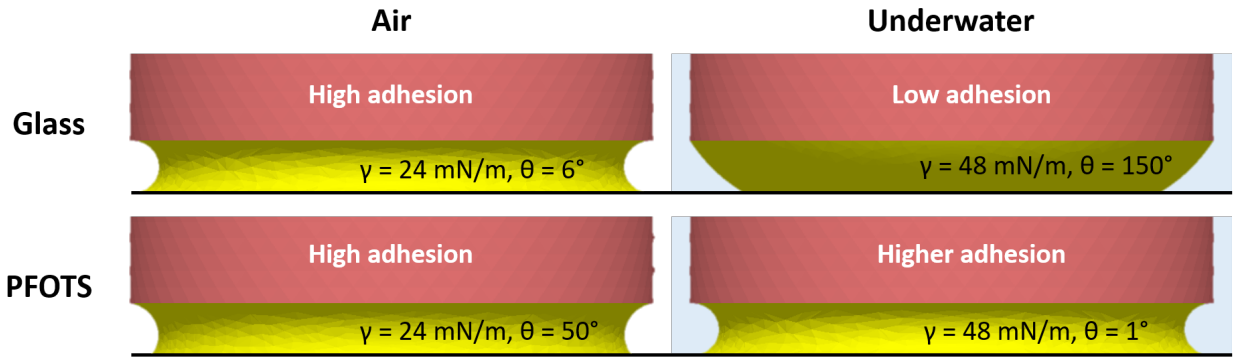

Figure 6: Simulation snapshots of oil capillary meniscus in contact with glass and PFOTS in air and underwater conditions. The corresponding interfacial tension, γ, and contact angle, θ, used to predict the ladybug's adhesion are labeled for each case.

The net force in the *underwater: bubble* case mainly depends on the proportion of hairs inside and outside the bubble (equation (**??**)). For the given bubble volume, only part of the hairs are inside the bubble for the hydrophilic substrate, while, all the hairs are inside the bubble for the hydrophobic substrate. Therefore, the force curve lies between *in air* and *underwater: no bubble* cases for a hydrophilic substrate, and closely follows the *in air* case for a hydrophobic substrate.

We see that the bubble itself doesn't contribute much to the net force on either substrate (Figure **??**). Its contribution even is slightly repulsive on the hydrophilic substrate due to the positive curvature of the bubble, and slightly attractive on the hydrophobic substrate due to its negative curvature. This small contribution is manifested by the slightly higher adhesion for *underwater: bubble* relative to *in air* for the hydrophobic substrate, since all

hairs are within the bubble in this case.

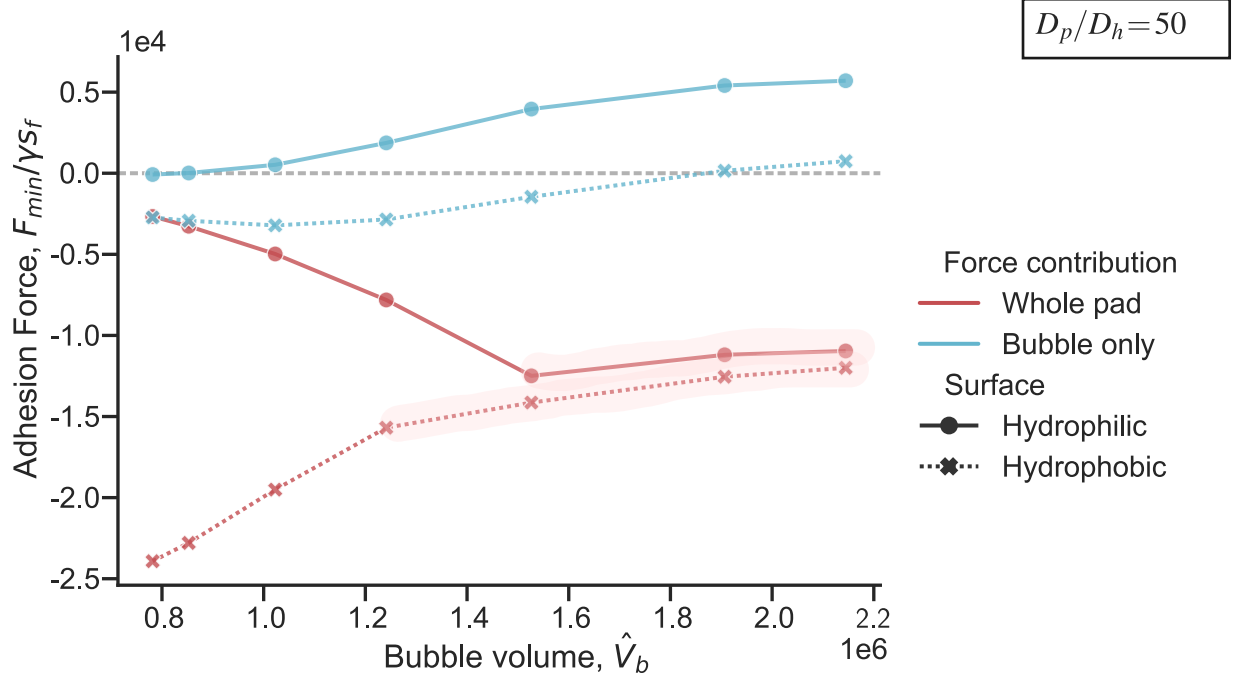## 3.4 Effect of bubble volume

Figure 7: Normalized adhesion force of a hairy pad system as a function of bubble volume, $\hat{V}_b$, for the *underwater: bubble* contact type. Adhesion forces are calculated from the minima of the respective force-distance curves. Negative force value represents attraction. Pad to hair diameter ratio (D_p/D_h) is kept fixed. Highlighted regions represent entrapment of all hairs within the bubble.

The volume of the bubble can influence its capillary force contribution, as well as change the relative proportion of hairs inside and outside it. To investigate this, we varied the bubble volume, $\hat{V}_b$, and compared the maximum adhesion force on both hydrophilic and hydrophobic substrates (Figure **??**). The contribution of the bubble to the net adhesion force is small regardless of its volume, when compared to the whole pad. Further, opposite trends of adhesion is seen on the two substrates with changing $\hat{V}_b$.

From previous section, we know that on the hydrophilic substrate, fluid bridges outside the bubble show poor adhesion due to the positive curvature of their meniscus. Thus, decreasing $\hat{V}_b$ decreases the adhesion force due to a larger proportion of hairs being outside

19

the bubble. In contrast, on the hydrophobic substrate, fluid bridges outside the bubble show higher capillary forces, due to its low contact angle and high interfacial tension in water. Thus, adhesion force increases for a hydrophobic substrate as the bubble size decreases.

A smaller $\hat{V}_b$ results in increased, but small, attraction by the bubble on both types of substrates. For larger values of $\hat{V}_b$ however, the force trend for the whole pad mostly follows that of the bubble. This is because the bubble gets big enough to entrap all the hairs inside it. Thus, the force contribution due to the fluid bridges remain unchanged, and only the bubble's contribution drives the slight variation in the pad's adhesion at high $\hat{V}_b$. Once the bubble is small enough such that part of the fluid bridges start making contact in water, the force trend changes, with a steep decrease (increase) in adhesion force on hydrophilic (hydrophobic) substrate as the volume decreases.
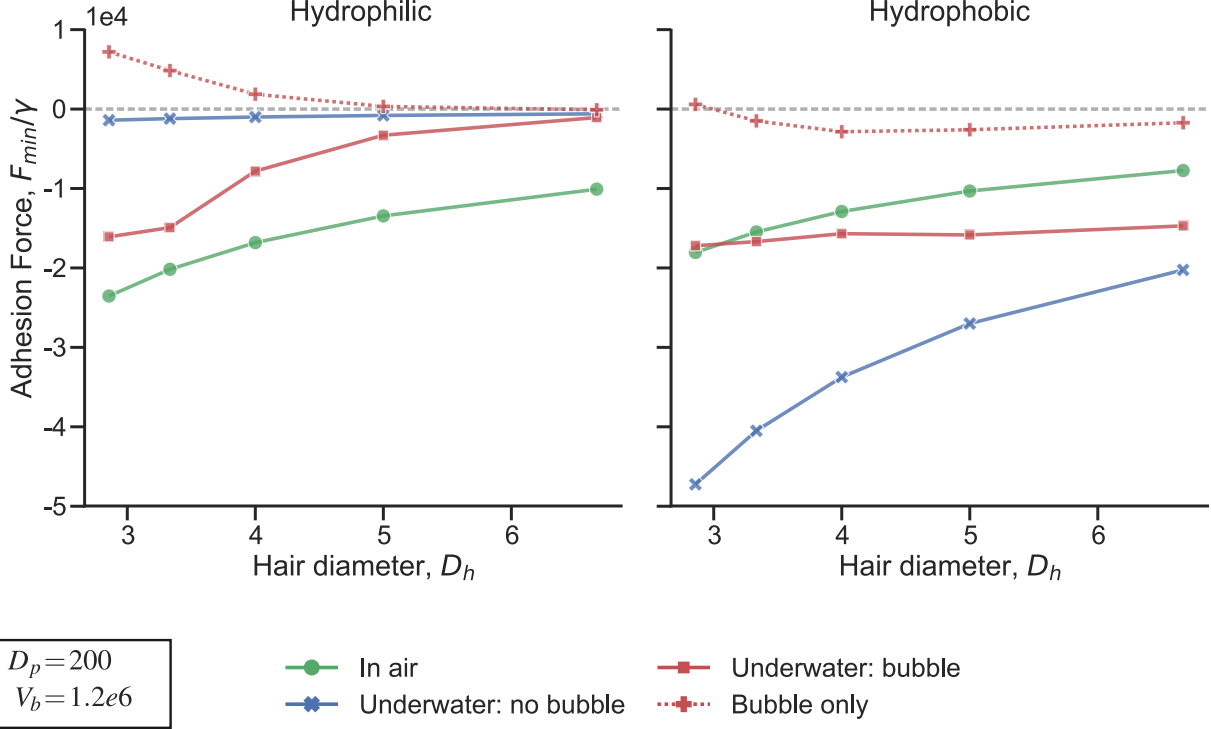
3.5 Effect of hair diameter

Figure 8: Normalized adhesion force of a hairy pad system on a hydrophilic and hydrophobic substrate as a function of hair diameter, D_h. Volume of each fluid bridge, V_f, scales relative to D_h based on the parameter $\phi_f = 2$. Adhesion forces are calculated from the minima of the respective force-distance curves, based on the capillary bridge model. A negative value represents attraction. The bubble's contribution to the net force for an *underwater: bubble* contact is denoted by plus symbols. Pad diameter and bubble volume are kept fixed. All lengths are scaled relative to D_p.

Hairs on a ladybug's pad terminate in various shapes like "discoidal" or "pointed". We studied this geometric effect on adhesion by changing the hair diameter, D_h (Figure **??**). Here, the pad diameter, total hair contact area and bubble volume are constant since D_p, α and $\hat{V}_b$ are kept fixed. The adhesive fluid volume is again assumed to scale relative to the hair diameter ($\phi_f = 2$).

Adhesion force increases with decreasing D_h for both hydrophilic and hydrophobic substrates in all contact types. This is consistent with the "contact splitting" theory, which predicts higher adhesion when the contact is split into many small contact points[?]. Re-

ducing the hair diameter results in two competing effects: 1) capillary force due to a single fluid bridge decreases due to its smaller size and "self-similar" scaling assumption ($f \sim D_h$), which decreases the net force, and 2) total number of fluid bridges increases since the total hair contact area is assumed to be fixed ($N \sim 1/D_h^2$), which increases the net force. The second effect dominates, resulting in a higher adhesion force as D_h decreases.

Similar to the trend in Figure ??, contact *in air* shows the highest adhesion force on a hydrophilic substrate for the given range of hair diameters, while on a hydrophobic substrate, *underwater: no bubble* shows highest adhesion. *Underwater: bubble* contact shows intermediate adhesion between *in air* and *underwater: no bubble* contact types.

The bubble's contribution gets repulsive as hair diameter decreases for both substrates (Figure ??). Since the aspect ratio L/D_h is fixed (Table ??), decreasing the hair diameter also decreases its length. Since the bubble's volume is kept constant, it will then have a lesser space available to occupy between the pad and the substrate, This results in it bulging outwards near the pinned contact line on the top, causing repulsion.

4   Discussion

Our experiments demonstrate that the ladybug beetle can attach underwater to a hydrophobic substrate even without a bubble trapped around its hairs. A previous study[?] had hypothesized that a bubble is necessary for underwater attachment in beetles. This is, however, only true for hydrophilic substrates, where a trapped bubble can facilitate underwater adhesion due to the hairs making contact in a dewetted environment. For a hydrophobic substrate, the adhesion is similar regardless of whether the contact occurs in air or underwater conditions, with or without a trapped bubble. Our theoretical calculations further show that the bubble by itself has a negligible capillary contribution to the net underwater adhesion of the pad. Direct force measurement of a single similarly sized bubble making contact with a hydrophobic substrate shows a maximum adhesion less than 50 μN, which

further validates that the bubble's contribution is insignificant (**??**).

Predictions of the ladybug's adhesion from the capillary bridge model agree with our experimental results (Figure **??**). In underwater conditions without a trapped bubble, adhesion on a hydrophobic substrate is significantly larger than on a hydrophilic substrate. This is explained by the different oil interfacial tension and contact angles with the substrates in air and underwater, which determines the capillary adhesive force in each case (Figure **??**). However, the experiments don't show the predicted ~ 2.6 times increase in underwater adhesion relative to that in air on the hydrophobic PFOTS surface. This discrepancy could be due to our assumptions of the oily fluid's interfacial properties. If we choose $\gamma_{fa}=30$ mN/m and $\gamma_{fw}=40$ mN/m, the corresponding increase in adhesion will be ~ 1.7, closer to our experimental value of ~ 1. The resulting change in θ_{fa} and θ_{fw} will further decrease this number. Direct measurement of the fluid's interfacial properties is thus essential to better predict the insect's adhesion, and will be a subject of future study. Further, due to surface inhomogeneities, not all the hairs might be able to completely drain the interfacial water layer, in order for the adhesive fluid to make a direct contact with the substrate. This can further reduce underwater adhesion, in comparison to our theoretical predictions which assumes a perfect contact.

In the model, we assume that all the hairs detach simultaneously to give a theoretical maximum achievable adhesion force. In our experiments, however, the pad always makes contact with the substrate at a random orientation, which is difficult to control precisely. During detachment, the pad typically peels off from its proximal to distal end rather than detach simultaneously. Our model also assumes the hairs to be of similar geometry, unlike the beetle's pad which has a distribution of flat or pointed tipped hairs. Thus, it's not surprising that the model overestimates the adhesion forces. The predictions are however in the same order of magnitude as experiments, and the qualitative trend is consistent for both hydrophilic and hydrophobic substrates in air and underwater.

Our study provides further validation that capillary forces by the adhesive fluid control

the insect's adhesion and van der Waals contribution, if any, must be negligible. Further, the capillary forces can even enable insect attachment underwater depending on the substrate chemistry. When underwater, without a trapped bubble, the pad adheres strongly to a hydrophobic substrate, but poorly to a hydrophilic substrate, even though it shows similarly strong adhesion to both substrates in air. This behavior can only be explained by capillary forces. Our preliminary FDMS results further provides validation to our assumption that the adhesive fluid can form capillary bridges with the substrate in water, instead of getting washed away (Table **??**).

The findings can also be extended to other animals relying on oily secretions for adhesion. Ants, for example, show similar adhesion on hydrophobic substrates under wet and dry conditions[?] , similar to what we see in a ladybug. Recent adhesion experiments on geckos reveal that they can attach well to fluoropolymer substrates underwater while they show little adhesion to the same substrate in air[?][?] . Geckos are thought to rely on van der Waals forces via dry contact with the substrate[?] , although recent observations of phospholipid footprints left behind walking geckos[?] could change that picture. Since geckos adhere poorly to PTFE (surface energy ~ 20 mN/m) one can speculate that the phospholipid material has a higher surface energy, and consequently makes a higher contact angle with PTFE in air. Let us assume the phosopholipid substance to be a fluid similar to oil with γ_{fa}= 30 mN/m and γ_{fw}= 42 mN/m such that its contact angle with PTFE is 80°. Equation **??** then gives us an underwater contact angle of 70° for the phospholipid fluid. Thus, on a PTFE surface, the capillary bridge model can predict a higher adhesion underwater than in air due to its lower contact angle and higher interfacial energy underwater. Based on similar assumptions, we predict the net adhesion force for the gecko on different substrates (Figure **??**). The adhesion force predictions are in good qualitative agreement with the whole animal experimental shear force values reported for the gecko, with the trend of higher adhesion in air than underwater for glass, similar adhesion in air and underwater for PMMA/OTS-SAM and lower adhesion in air than underwater for PTFE. We, thus, propose that the underwater

experiments performed on geckos[?][?] indicate a capillary contribution to gecko adhesion. We suggest performing single seta adhesion force tests similar to Autumn et. al.[?] using a hydrophilic and fluorinated probe in air and underwater conditions to validate the role of capillary contributions to gecko adhesion.
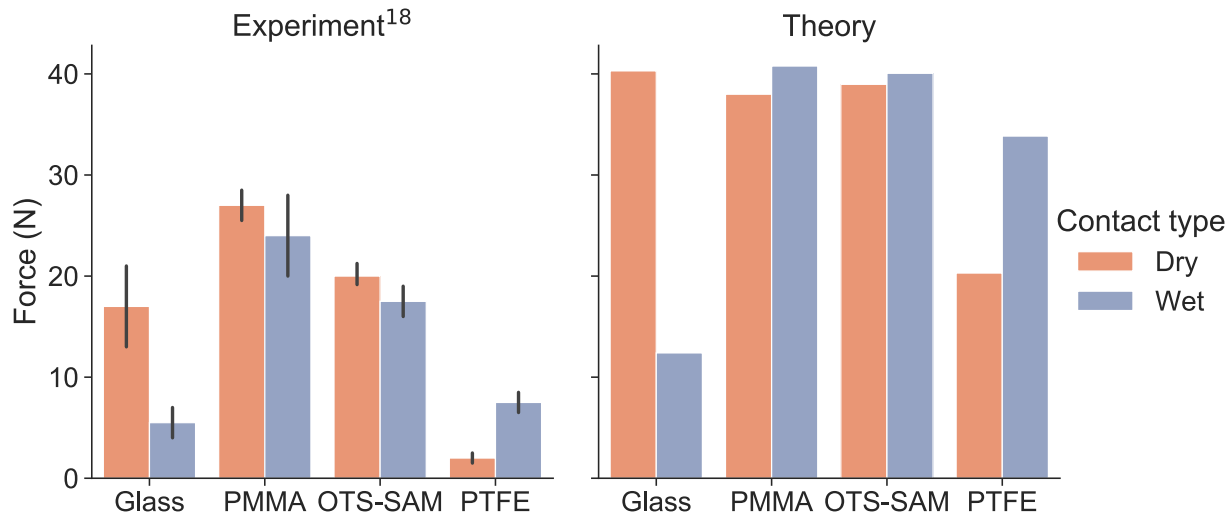

Figure 9: Whole animal adhesion force of geckos on various substrates. Experimental shear adhesion values are reproduced from Stark et. al.[?] . Normal adhesion forces for each gecko toe are theoretically estimated from the capillary bridge model, with hair diameter = 400 nm, toe diameter = 4 mm, adhesive fluid volume = 4.19×10^{-3} fL and 10% hair coverage. "*Underwater: no bubble*" type contact is assumed for the "Wet" case. Net adhesion force is calculated by assuming 5 toes on each leg and 4 legs in total on a gecko. Interfacial tension of the phospholipid layer (PL) in air and water are assumed to be 30 mN/m and 42 mN/m respectively. PL contact angles with glass, PMMA, OTS-SAM and PTFE are assumed to be 6°, 10°, 20° and 80° respectively. The corresponding water contact angles are 50°, 85°, 94° and 97° respectively, as reported in Stark et. al.[?] .

We have so far limited our analysis to only smooth substrates. Insects in the real world, however, interact with rough substrates very often. Previous studies[?] have shown that substrate roughness is a more dominant parameter than substrate chemistry in controlling insect adhesion. Future work will explore how roughness can impact the net capillary force. Our study can have potential applications in the design of bio-inspired materials to achieve underwater adhesion via capillary bridges. Bubble can possibly be used to control underwater adhesion by changing the relative proportion of the arrays inside and outside the bubble. A

suitable choice of adhesive fluid can be made tailored to the substrate and environment of application to achieve optimal adhesion performance.

5 Conclusions

Ladybug beetles rely primarily on their oily fluid secretion to adhere to surfaces in both air and underwater conditions. The beetle can attach underwater on a hydrophobic substrate even without a trapped air bubble within its hairy pad, although it loses this ability on a hydrophilic substrate. This is explained theoretically by the different contact angle and interfacial tension of the adhesive fluid in air and underwater conditions. Further, the bubble itself has a negligible capillary contribution to the total force. The trapped bubble can promote adhesion only on a hydrophilic substrate by providing an air medium to the adhesive fluid bridges inside it. Oil wettability, thus, primarily controls the insect's adhesion in any given condition. A similar argument also explains previously reported underwater measurements in geckos[?], which highlights the possibility of capillary contributions to gecko adhesion. Future studies should characterize the fluid secretion's interfacial properties with a particular substrate to better understand the nature of the animal's adhesion.

6 Acknowledgement

A Appendix

A.1 Simulation method: Single capillary bridge

Capillary force due to a single adhesive fluid or bubble meniscus (termed "capillary bridge") is calculated by performing simulations in Surface Evolver[?], similar to the method described by De Souza et. al.[?]. A simple cubic geometry, mimicking the capillary bridge, of constant volume, V, is defined as the initial condition with an interfacial tension, γ, with the surrounding medium. Interfacial tension of the capillary bridge with the substrate is given by $\gamma \cos \theta$, where θ is the corresponding contact angle inside the bridge. For the case of a bubble meniscus, θ is defined w.r.t. the surrounding water, since θ can also directly characterize the substrate wettability. The capillary bridge spans a gap distance d between the top face and the substrate. The boundary conditions are set corresponding to a pinned contact line of diameter D on the top face and constant interfacial tension with the substrate on the bottom. All lengths are normalized relative to length $s = (3V/4\pi)^{1/3}$. An appropriate geometry refinement routine is chosen to evolve the capillary bridge shape to its minimum energy state. The normalized total capillary force, $\hat{f} = f/\gamma s$, is the sum of the Laplace pressure and surface tension contributions , where:

$$f = f_{laplace} + f_{surface\,tension} = \Delta P_{laplace} A_{bottom} + 2\pi R_{bottom} \gamma \sin \theta \tag{A.1}$$

Here, $\Delta P_{laplace}$ is the Laplace pressure of the equilibrium capillary bridge, A_{bottom} is the contact area of the capillary bridge with the substrate at bottom and R_{bottom} is the corresponding radius of contact, all obtained from the simulation output for the equilibrium surface.

The gap distance d is varied stepwise and the capillary force is calculated each time to obtain force-distance curves for a particular choice of D and θ.

A.2 Single capillary bridge: Effect of volume

Surface Evolver simulation results showing the effect of volume on the maximum capillary force of a single fluid bridge. Since the fluid is pinned at the top to the same diameter, D, a smaller volume would result in high interfacial curvatures, which increases the capillary force due to the negative Laplace pressure. In this case, small contact angles lead to a greater increase in adhesion.
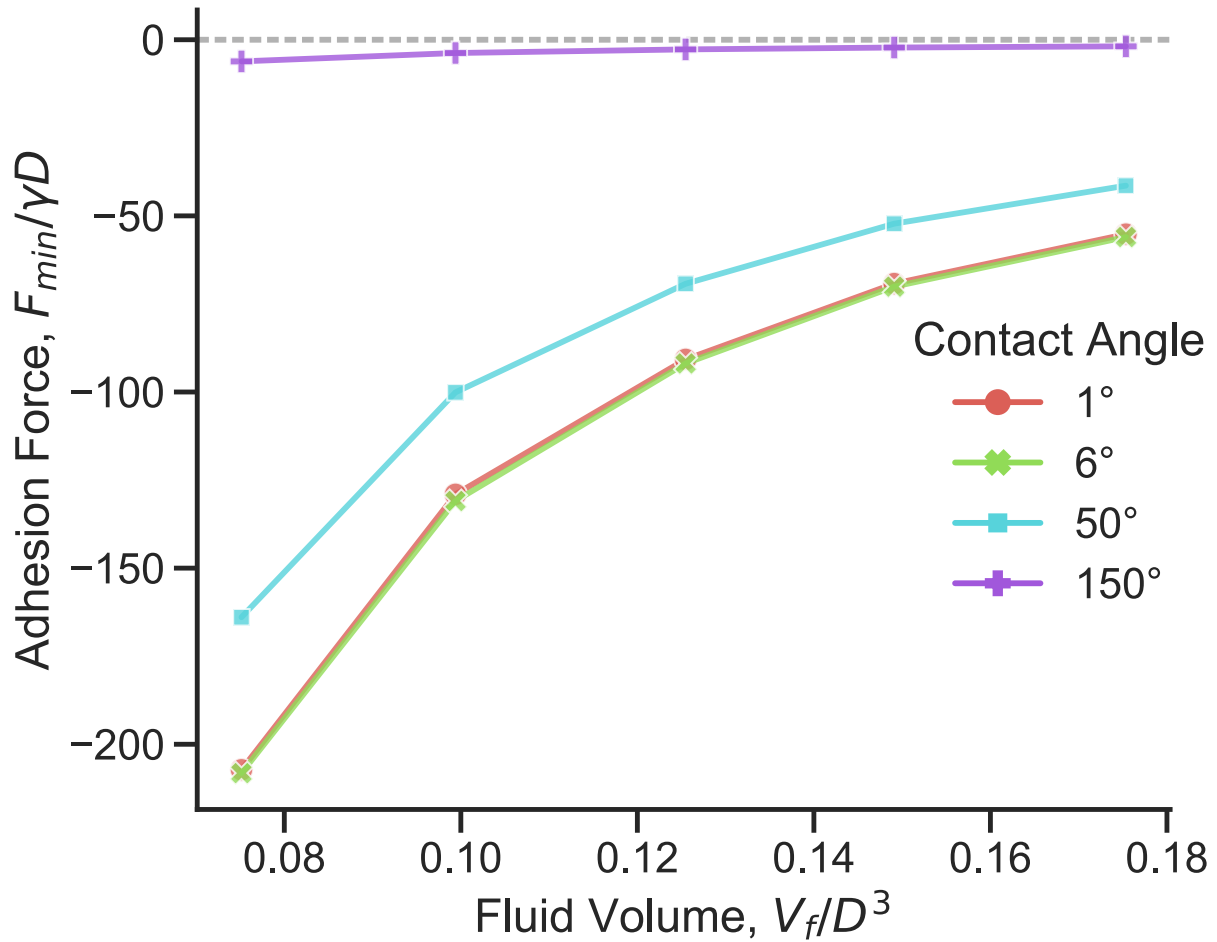

Figure A.1: Normalized maximum capillary force for a single bridge as a function of fluid volume

A.3 Capillary Bridge Model: Effect of hair diameter at constant fluid volume

Here, instead of scaling the fluid volume relative to the hair diameter, we now assume a fixed total fluid volume distributed equally among the N hairs. Total fluid volume, $V_{total} = NV_f = 2000$. Hair diameter is varied while keeping the total hair contact area constant. Length is in arbitrary units. Forces increase at a much smaller rate on decreasing diameter when compared to the case with self-similar scaling of fluid volume (Figure **??**).
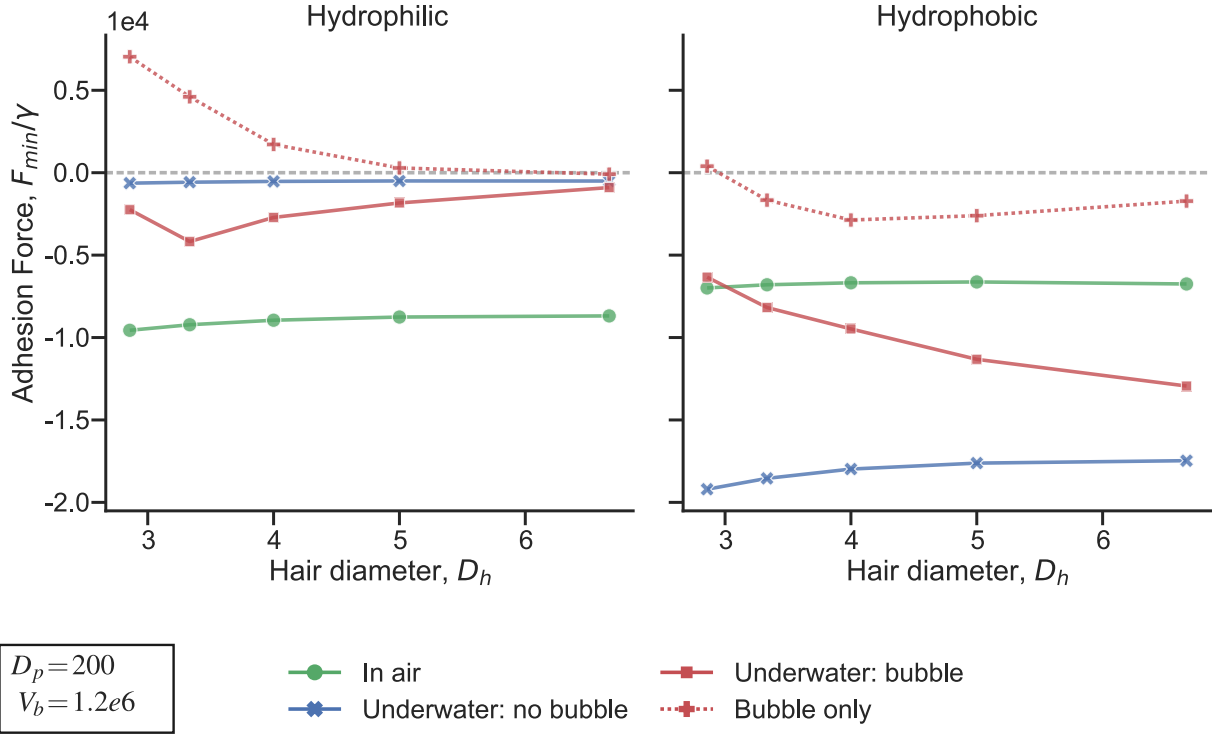

Figure A.2: Normalized adhesion force of hairy pad system on a hydrophilic and hydrophobic substrate as a function of hair diameter (D_h), calculated from the capillary bridge model. The total adhesive fluid volume is fixed to 2000. Adhesion forces are calculated from minima of the respective force-distance curves. Negative force value represents attraction. The bubble's contribution to the net force for an *underwater: bubble* contact is denoted by plus symbols. Bubble volume and pad diameter are kept fixed. All lengths are scaled relative to D_p.

A.4 Statistical comparison

Pairwise statistical comparison of single leg adhesion force measurements of the ladybug beetle (*Coccinella septempuctata*) for each contact type and substrate are shown (Table **??**). The uncorrected p-values and Common Language Effect Size (CLES) are obtained from post-hoc pair-wise Student t-test between A and B while keeping the third parameter fixed. p-values showing statistically significant difference between A and B are in boldface. The condition for statistical significance is based on the Bonferroni-corrected critical p-value of 0.008.

Table 4

Fixed	A	B	p-value	CLES
In air	PFOTS	Glass	0.959	0.48
Underwater: bubble	PFOTS	Glass	0.011	0.96
Underwater: no bubble	PFOTS	Glass	$< \mathbf{0.001}$	1.0
PFOTS	In air	Underwater: bubble	0.897	0.48
PFOTS	In air	Underwater: no bubble	0.828	0.48
PFOTS	Underwater: bubble	Underwater: no bubble	0.721	0.44
Glass	In air	Underwater: bubble	**0.002**	1.0
Glass	In air	Underwater: no bubble	$< \mathbf{0.001}$	1.0
Glass	Underwater: bubble	Underwater: no bubble	0.07	0.84

A.5 Capillary force due to a bubble

Capillary force of a single bubble against a PFOTS surface are compared for two different volumes. The volumes correspond to the expected range in the case of the trapped bubble in a ladybug. Here, the bubble is pinned to a micropatterned PDMS substrate on the top. The maximum adhesion force of any of the bubble never exceeds 50 µN, significantly lower

than the beetle's underwater adhesion to the same substrate ($> 400\ \mu$N). Thus, the bubble's contribution to adhesion in the "*underwater: bubble*" contact of a ladybug's pad should be negligible.
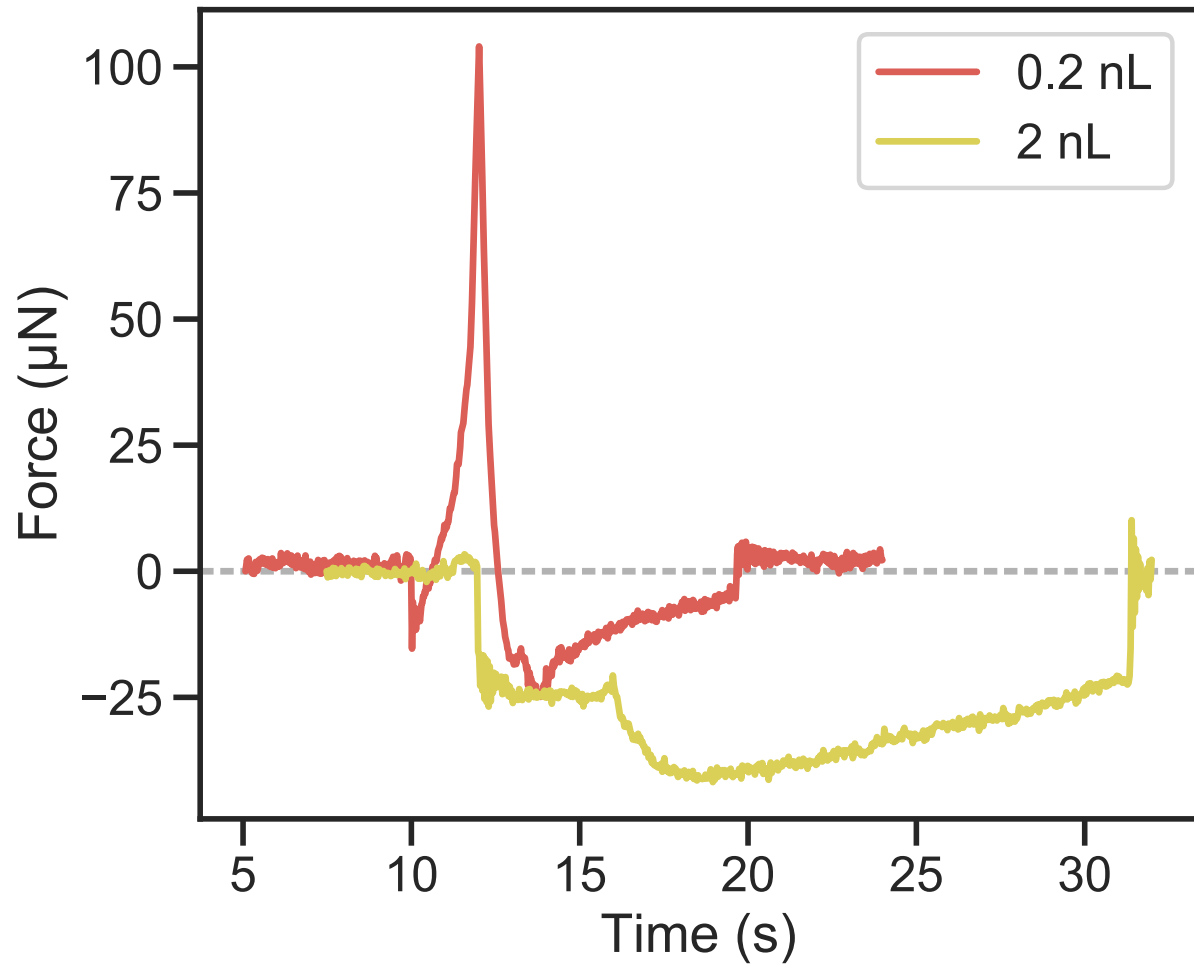

Figure A.3: Capillary force of the bubble